Desalination and Water Treatment
www.deswater.com
doi: 10.5004/dwt.2019.23503

142 (2019) 371–380
February

Magnetic Fe-doping g-C_3N_4/graphite: the effect of supporters and the performance in Fenton-like reactions

Jianqing Ma[a], Ziheng Huang[b], Hao Xi[b], Yuezhong Wen[a,*]

[a]*Institute of Environmental Health, College of Environmental and Resource Sciences, Zhejiang University, Hangzhou 310058, China, Tel./Fax: +86 571 88982421; emails: wenyuezhong@zju.edu.cn (Y. Wen), 1096224278@qq.com (J. Ma)*
[b]*College of Biological and Environmental Engineering, Zhejiang Shuren University, Hangzhou 310015, China, emails: 583015633@qq.com (Z. Huang), 912531941@qq.com (H. Xi)*

Received 2 March 2018; Accepted 21 November 2018

ABSTRACT

Metal-doping graphitic carbon nitride (g-C_3N_4) is a potential catalyst for the Fenton-like reaction. Selecting an appropriate supporter for this material is essential to improve its catalytic ability and lower the costs. Three common supporters, graphite, activated carbon, and SBA-15, were employed to investigate their effects on the catalyst structure and performances. Results show that graphite could increase the active Fe–N centers due to geometric effects and promote the electron transfer by π–π stacking, and therefore, the Fe-doping g-C_3N_4/graphite (FegN/G) composite displayed excellent catalytic ability for the bisphenol A (BPA) removal. In addition, magnetic catalyst was further fabricated through a simple coprecipitation method using Fe_3O_4 and chitosan-Fe hydrogel. The magnetic catalyst kept in dozens of micrometer size range as well as high activity for the Fenton reaction. Hydroxyl radicals were generated during the reaction process, and 99.9% of the original BPA was therefore degraded and mineralized in 1 h. More importantly, it also exhibits a good reusability and stability, as well as a quick separation performance from the solution when using a magnet, indicating that this magnetic FegN/G composite would be a promising Fenton-like catalyst in practical applications.

Keywords: Graphitic carbon nitride; Fenton-like reaction; Magnetic separation; Catalyst

1. Introduction

Recently, graphitic carbon nitride (g-C_3N_4) has gained tremendous attention in the field of photocatalysts due to its unique electronic structure, good physicochemical stability, as well as facile and low-cost preparation [1–3]. Many modification studies have been carried out to enhance its catalytic ability and consequently broaden the application domain of these g-C_3N_4-based materials. There into, transition metal doping is an effective strategy to introduce the metal-N moieties, which play crucial roles in some reactions such as selective oxidation of benzene [4], N_2 photofixation [5], and oxygen reduction reaction [6]. It is reported that the doped Fe can be embedded and stabilized at the interstitial position of the g-C_3N_4 sheets through Fe–N coordination [7], forming structures much similar to that in metalloporphyrins, and thus can participate in the H_2O_2 activation [8]. Therefore, such materials could be used as potential Fenton-like catalysts for the organic contaminant control, in which powerful hydroxyl radicals (HO·) are produced alongside the Fe(II)/Fe(III) cycle.

Based on this, our group has prepared the Fe-doping g-C_3N_4/graphitized mesoporous carbon (GMC) composite and used as an efficient Fenton-like catalyst at a wide pH range [9]. Its vigorous catalytic ability originates from the complexation of iron by g-C_3N_4 and the cooperation with GMC through π–π stacking and thereby accelerates the redox cycle of Fe(II)/Fe(III). Though effective, two problems

* Corresponding author.

of this catalyst still remain as a stumbling block to its practical use. First, the price of the GMC precursor is still high at the present stage and a low-cost replacement is thereby needed. Second, the catalyst has small particle sizes ranging from several to dozens of micrometers, making it difficult to separate from the liquid. Magnetic separation is viewed as a selective and efficient method to deal with small particles in the solution [10]. By this means, catalysts can be easily separated from water with the help of magnetic field while keep high catalytic ability [11,12]. Therefore, a magnetic Fe-doping g-C_3N_4-based Fenton-like catalyst with lower cost is aimed to fabricate.

The study starts with selecting of the appropriate supporter for Fe-doping g-C_3N_4. The use of a supporter will not only cut down the catalyst loading due to the dispersion effect but also influence the catalyst activity through the geometric effect and electron interactions and thereby modify the number and activity of active sites on the catalyst surface [13,14]. Herein, we studied the effect of three supporters, graphite, activated carbon (AC), and SBA-15, on the performance and structure of the prepared catalysts. Graphite is a commonly available carbon material and can act as a heterogeneous catalyst for the activation of H_2O_2 in the organic oxidation process [15]. It is believed that charge transfer can happen between metal and graphite, as plenty of delocalized π-electrons exist on the graphite surface [16,17]. And it proved to be an excellent supporter for the preparation of Fe-doping g-C_3N_4 graphite (FegN/G) composite. Next, a facile coprecipitation method modified from our previous work [18], using chitosan-Fe hydrogel to combine Fe_3O_4 and FegN/G at the same time, was applied. The obtained magnetic catalyst also showed excellent performances in the bisphenol A (BPA) degradation, a well-known endocrine disruptor detected in many industrial effluents [19]. What's more, it can be easily separated from the solution when using a magnet, indicating this magnetic FegN/G composite would be a promising Fenton-like catalyst in practical applications.

2. Experimental

2.1. Chemicals and Reagents

Dicyandiamide (DCD, Chemical pure (CP), 98%), hydrogen peroxide (guaranteed reagent, 30% w/w), BPA (CP), $FeCl_3{\cdot}6H_2O$ (analytical reagent (AR), 99%), and Na_2SO_4 (AR, 99%) were obtained from National Medicines Corporation Ltd. of China. Chitosan with a deacetylation degree of 91.2% was supplied by Zhejiang Golden-Shell Biochemical (Zhejiang, China). Graphite (4,000 mesh, 99.95%) was purchased from Aladdin Industrial Corporation, China. Mesoporous silica SBA-15 ($SiO_2/Al_2O_3 \geq 500$) and AC (200 mesh) were purchased from Nanjing XFNano Material Tech Co., Ltd., and Qingdao Guanbaolin Huoxingtan Co., Ltd, China, respectively. Other chemicals were of laboratory reagent grade and used without further purification. The deionized water used in this study was produced using a UPK/UPT ultrapure water system.

2.2. Preparation of magnetic FegN/G

The first step was to prepare FegN/G composite. Specifically, 1 g of DCD was dissolved in 20 mL deionized water, followed by the addition of 0.2027 g $FeCl_3{\cdot}6H_2O$ at 80°C and stirring for 1 h. Then, 0.2 g graphite was added to this solution. The mixture was continually stirred at 120°C until water was completely evaporated. The dried mixture was grinded and heated to 600°C in a nitrogen atmosphere with a rate of 10°C/min and kept for 3 h, and the obtained powder was named as FegN/G. SBA-15 and AC were also used instead of graphite for reference, which were denoted as FegN/SBA-15 and FegN/AC, respectively.

Next, FegN/G was combined with magnetic Fe_3O_4 using chitosan-Fe hydrogel via a coprecipitation method. A 0.25 g chitosan was first dissolved in 50 mL of 0.025M $FeCl_3$ aqueous solution. Then, 1 g FegN/G and 0.025 g Fe_3O_4 synthesized through a solvothermal method [20] were added to the mixture which was further stirred for 2 h. After this, an adequate amount of Na_2SO_4 solution (0.1 mol/L) was dropped, and all the components were precipitated. The solid was collected by a magnet and washed with water for several times. Finally, it was dried at 60°C and denoted as M-FegN/G.

2.3. Characterization methods

The specific surface area was calculated by Brunauer-Emmet-Teller equation according to the N_2 adsorption isotherms at 77°K on a NOVA2000e surface area and pore size analyzer (Quantachrome, USA). The surface structure and morphology were observed with a SIRION 200 scanning electron microscope (SEM, FEI, Netherlands) and a Jem1200 transmission electron microscope (TEM, JEOL, Japan), while energy-dispersive X-ray spectroscopy (EDS) gave the element analysis of the samples. Fourier transform infrared spectroscopy (FTIR) of the KBr pelleted samples were recorded on AVATAR 370 FTIR spectrometer (Thermo Nicolet, USA) over the wavenumber range 400–4,000 cm^{-1}. X-ray diffraction (XRD) spectra were collected on a XRD-6000 X-ray diffractometer (Shimadzu, Japan) with a Cu Kα radiation (λ = 1.5406 Å) over a 2θ range of 10°–60°. X-ray photoelectron spectroscopy (XPS) was collected on an ESCALAB 250Xi spectrometer (Thermo Scientific, UK) with a monochromatic Al Kα source (1,486.6 eV), and all binding energies were referenced to the C 1s peak at 284.2 eV. X-ray adsorption near-edge structure (XANES) of Fe K-edge was measured using a transmission mode at the 14W1 beamline of the Shanghai Synchrotron Radiation Facility (SSRF). The magnetization curve was measured by a J3426 Vibrating sample magnetometer (Cryogenic, UK).

2.4. Performance tests of the catalysts

The degradation of BPA was performed with an initial concentration of 20 mg/L (pH = 6.8) and a volume of 50 mL. For each experiment, 200 μL H_2O_2 and a certain amount of the catalyst were added into the flask, which were then agitated at 150 rpm in a thermostatic shaker and maintained at 25°C. At desired intervals, proper solution was taken out and filtered through a 0.22 μm syringe filter. Then, 1.0 mL of the supernatant was immediately mixed with 10 μL of *tert*-butanol and subjected to a Waters® e2695 reverse-phase high performance liquid chromatography (HPLC) coupled with a Waters® 2998 photodiode array detector (Milford, MA, USA). The BPA concentration was determined at 224 nm. The organics were separated by a Waters®

XBridge™ Phenyl column (250 mm × 4.6 mm, 5 mm), and the temperature was kept at 25°C. The mobile phase was the mixture of 70% methanol and 30% water, with a flow rate of 0.8 mL/min. The concentration of formic acid produced at the degradation process was also measured by HPLC using a Waters®Atlantis™ T3 column (250 mm × 4.6 mm, 5 mm) at 210 nm and 30°C. The mobile phase was 10 mmol/L NaH_2PO_4 aqueous solution (adjusting pH to 3.0 with H_3PO_4) with a flow rate of 0.5 mL/min.

At the end of the degradation process, M-FegN/G was separated with a magnet and then put into another cycle of use. The concentrations of leaching iron were measured by an AA800 atomic absorption spectrophotometer (PerkinElmer, USA). Total organic carbon (TOC) was determined by a Multi N/C 3100 TOC analyzer (JENA, Germany). The H_2O_2 consumption tests by different catalysts were carried out in a 50 mL of 40 mM H_2O_2 solution. The concentration of H_2O_2 was measured by spectrophotometric determination using titanium sulfate method [21] on a UV-2410 UV-Vis spectrometer (Shimadzu, Japan) at 400 nm.

Electron spin resonance (ESR) signals of the radicals trapped by 5,5-Dimethyl-1-pyrroline N-oxide (DMPO) were obtained on a BRUKER A300 electron paramagnetic resonance spectrometer. The settings were center field 3,514.3 G, microwave frequency 9.85 GHz, and power 20.27 mW.

3. Results and discussion

3.1. The effect of supporters on catalytic performances

Graphite with 4,000 mesh was first chosen as the low-cost carbon precursor, and the optimized dosage was 0.2:1 (graphite:DCD) according to Fig. S1. Clearly, the composition with graphite can greatly improve the catalytic ability of FegN, as the BPA removal efficiency increased from 19.0% to 99.0% (Fig. 1(a)), while the adsorption was only slightly increased from 9.0% to 15.5% (Fig. 1(b)) in 1 h. It is noticed that at 40 min, BPA removal by FegN/G has already reached to 95.4%, which was comparable with the performance of Fe-g-C_3N_4/GMC under the same conditions in our earlier report [9], manifesting that graphite with 4,000 mesh was a successful precursor for this Fenton-like catalyst.

To evaluate the effect of different supporters exerted on the Fe-doping g-C_3N_4, two common supporters for catalyst preparation, AC and SBA-15, were also employed in this study. The BPA removal in 1 h by FegN/AC and FegN/SBA-15 was 86.8% and 93.8%, respectively, which were much higher than FegN but still lower than FegN/G, confirming that graphite was the best choice for the FegN composite. In addition, Fig. 2 revealed that FegN/AC and FegN/SBA-15 caused a higher H_2O_2 consumption rate than FegN/G. Especially, for FegN/AC, H_2O_2 was almost depleted in 5 min, consequently leading to the small decrease of BPA concentration in the later process. Specific surface areas of FegN/G, FegN/AC, and FegN/SBA-15 are 27.8, 226.2, and 52.9 m^2/g, respectively. It seems that the catalytic ability of the catalyst is more sensitive to its chemical structure rather than the specific surface area. However, the specific surface area has a positive correlation with H_2O_2 consumption rate. In a Fenton-like reaction, H_2O_2 takes part in both the steps with the HO· as reduction products (reactive oxygen species for organic removal) and with $O_2^{\cdot}$ or O_2 as oxidation products [22]. Besides, direct decomposition of H_2O_2 to H_2O and O_2 could also happen [23]. It was reported that the decomposition of H_2O_2 to O_2 is highly related to the surface area [24,25], which implies that FegN/AC and FegN/SBA-15 can cause more O_2 production. Combining the results, it can be concluded that the increase of the specific surface area by AC or SBA-15 could enhance the total decomposition mostly by increasing the ineffective consumption of H_2O_2, while the reactive oxygen species production relies heavily on the chemical structure modified with the supporter during the synthesis process and the electron interactions with the supporter.

3.2. The effect of supporters on active sites

Further characterization methods were used to reveal the structure difference induced by these supporters. According to FTIR spectra in Fig. 3(a), FegN/G and FegN/SBA-15 keep

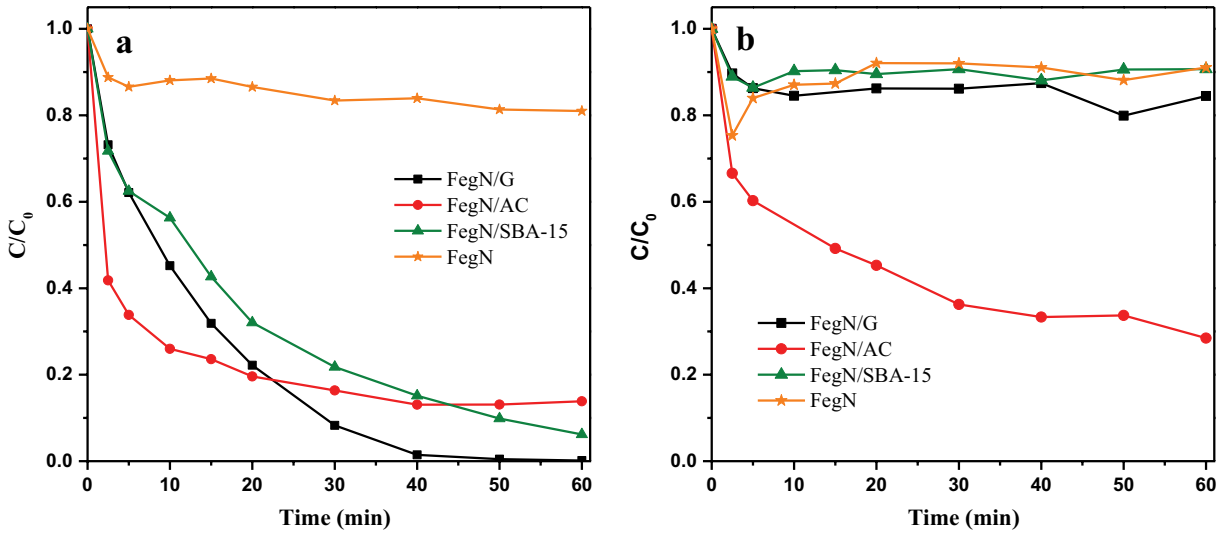

Fig. 1. Time profiles of BPA removal by (a) degradation using 40 mM H_2O_2 and (b) adsorption (BPA 20 mg/L, pH = 6.8, catalyst dosage 0.8 g/L, 25°C).

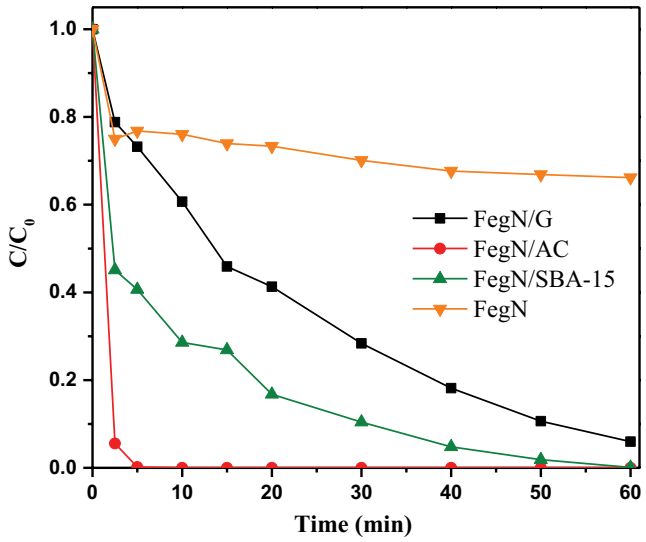

Fig. 2. Time profiles of H_2O_2 consumption by different catalysts (H_2O_2 40 mM, catalyst 0.8 g/L, 25°C).

the basic breathing mode of g-C_3N_4 at 806.5 cm^{-1} and stretching mode at 1,240–1,640 $cm^{-1}$of the tris-s-triazine, suggesting that graphite and SBA-15 act as scaffolds for the FegN sheet growth and thus improved its activity to a certain extent. After the inclusion of AC, however, the original C–N network was partially destroyed. For FegN/AC, the bands at 1,644 and 1,418 cm^{-1}, which correspond to the stretching vibration modes of heptazine-derived repeating units, disappeared. A dramatic decrease of the intensity is also observed at the g-C_3N_4 (002) peak (27.5°) from the XRD patterns in Fig. 3(b) and Fig. S2, indicating the disorder or the destruction of the FegN layers after combining with this carbon precursor. Fig. 4 illustrates the SEM images of these catalysts. Considering the two-dimensional property of the g-C_3N_4 layers, the geometric effect of the supporter may exist. During the synthesis process, the DCD was easily polymerized on the structured surfaces of the graphite and SBA-15. While for AC, due to the amorphous nature and irregular porous structure, the precursor could only form fragmentary layers on its surfaces.

For all these catalysts, Fe is still present in an amorphous form, as no crystalline species peak can be found. But confirmed by XPS results in Table 1, their surface chemical structure is clearly changed. The Fe/N atomic ratio of FegN/AC and FegN/G is much higher than FegN, suggesting a more stable Fe–N substructure originating from the chemical coordination or electron coupling between the carbon materials and FegN layers [6]. It seems that these carbon materials not only provide a framework for the growth of active sites during the pyrolysis process but also influence the chemical structure of the supported materials and consequently accelerate the electron transfer in the reaction process. Considering the similarity of the structure, this effect is inferred as the π–π stacking as reported in graphene [6,26,27] and GMC [9]. The high-resolution N 1s spectra in Fig. 5 are divided into two species: N in triazine rings (C–N–C)/N–Fe at 398.3 eV (two species lie close and cannot be exactly distinguished) and tertiary N (N–$(C)_3$) at 400.1 eV. C–N–C/N–Fe is the dominated species for all samples. The spectra of Fe 2p are divided into three species: Fe–N at 709.2 eV, FeO/Fe_3O_4 at 710.4 eV, and Fe_2O_3 at 711.5 eV. According to the deconvolution results listed in Table 1, FegN/G has the maximum Fe–N species (43.3%) compared with FegN and other samples. It has been proved that Fe–N centers of the FegN-based materials are the main active sites for the Fenton-like reaction [9], and this also explained the reason for FegN/G having the most active catalytic ability.

On the other hand, Fe K-edge XANES spectra show the difference in oxidation and bonding geometry of the doped Fe in a more direct way [28]. Iron phthalocyanine (FePc) and hematin are chosen as the reference compounds of Fe (II) and Fe (III). According to the adsorption edge position in Fig. 6, the oxidation state of Fe in FegN is close to +3. However, the local geometry is different from the hematin, as the much lower intensity of the pre-edge at about 7,113 eV (peak A) can be observed, which is relating the local symmetry of the central iron [29]. Clearly, it has no square-planar Fe–N_4

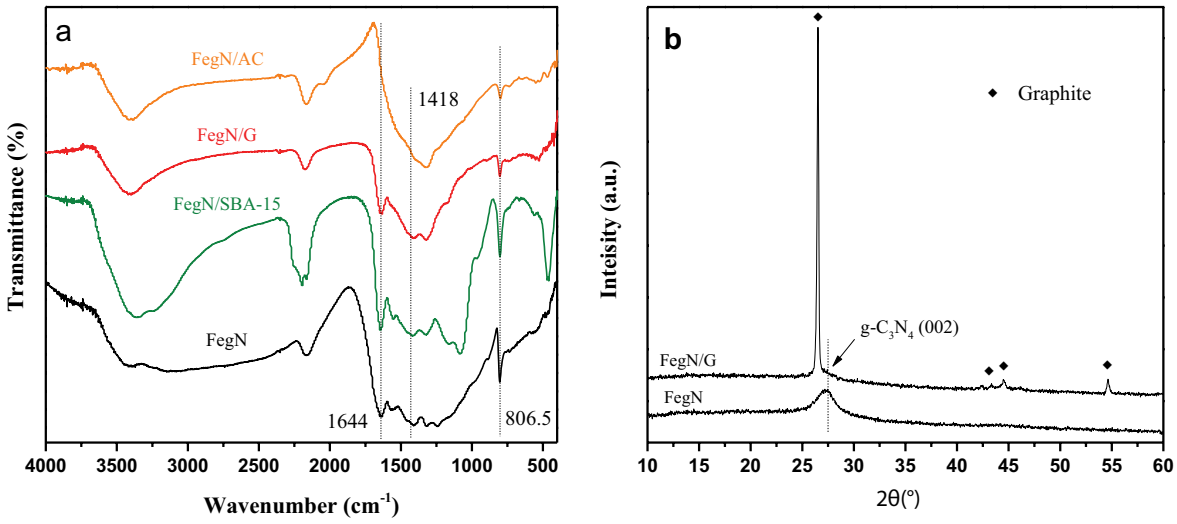

Fig. 3. (a) FTIR spectra and (b) XRD spectra of different samples.

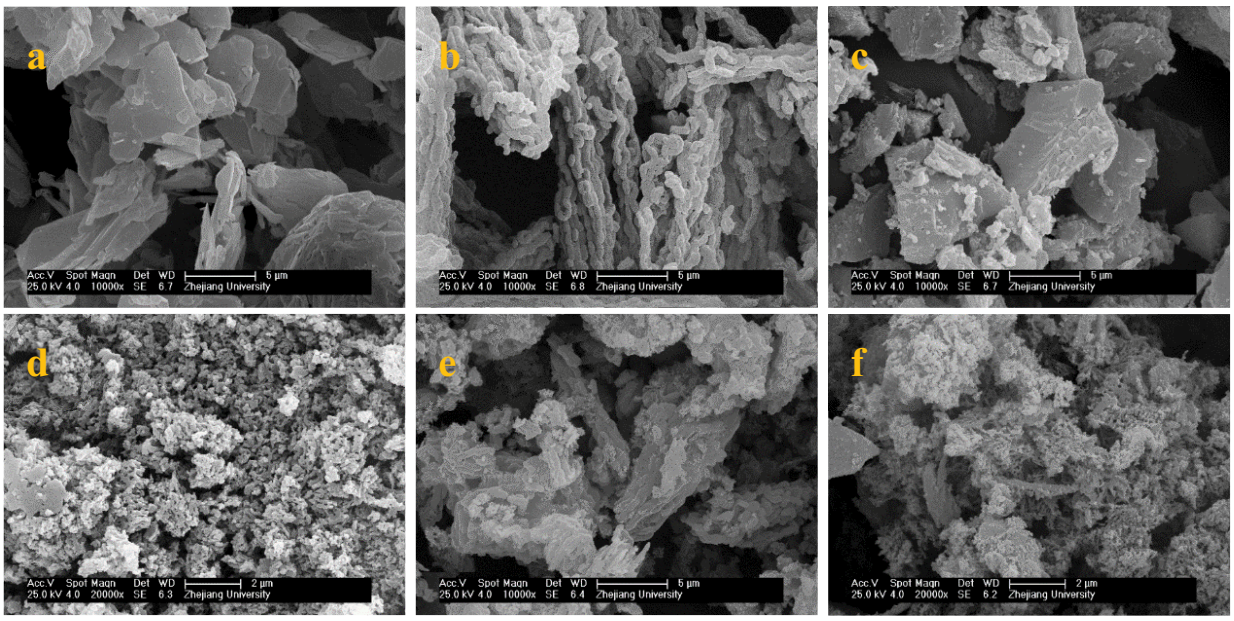

Fig. 4. SEM images of (a) graphite, (b) SBA-15, (c) AC, (d) FegN/G, (e) FegN/SBA-15, and (f) FegN/AC.

Table 1
Percentage contents of different N and Fe species in their total amounts calculated from the XPS results

Samples	C–N–C/N–Fe	Tertiary N	Fe–N	FeO/Fe_3O_4	Fe_2O_3	Fe/N
FegN	0.842	0.158	0.157	0.421	0.422	0.065
FegN/G	0.900	0.100	0.433	0.390	0.177	0.116
FegN/AC	0.946	0.054	0.365	0.250	0.385	0.175
FegN/SBA-15	0.847	0.153	0.365	0.264	0.381	0.078

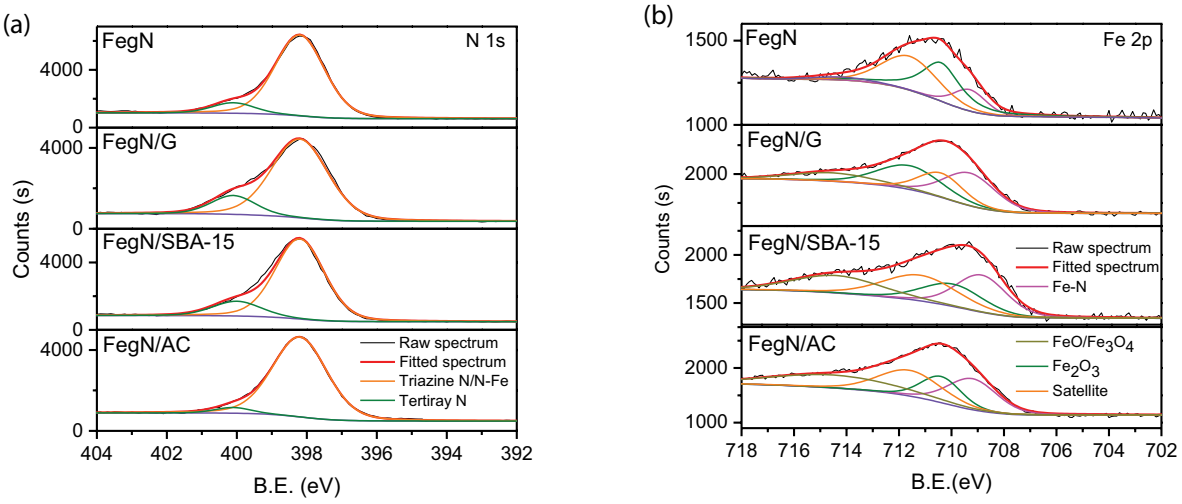

Fig. 5. Deconvolution profiles of (a) N 1s and (b) Fe 2p spectra of the prepared samples.

structure as in FePc (peak B at 7,117 eV). Ghosh et al. [7] used the density function theory and concluded that the Fe is almost symmetrically embedded in the g-C_3N_4 cavity through chemical coordination with the six nitrogen. After combining with graphite, the intensity of peak C (due to 1s to 4p transitions) decreased, indicating a more reduced state of iron compared with FegN caused by the interaction with graphite as electron donor [30]. By contrast, the peak C of

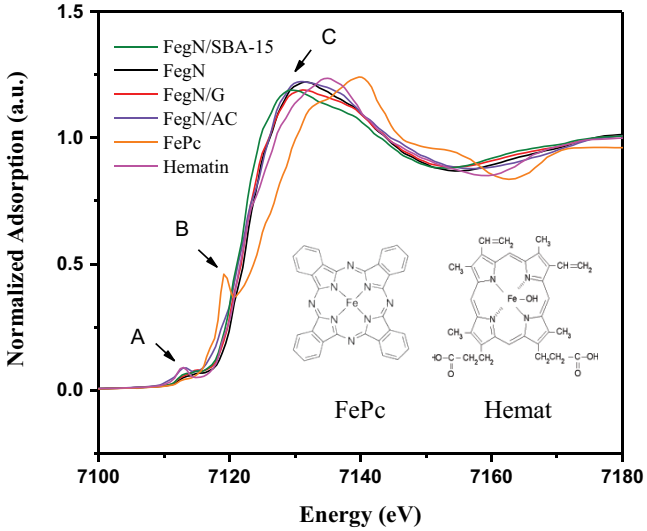

Fig. 6. Normalized Fe K-edge XANES spectra of the prepared samples and reference samples.

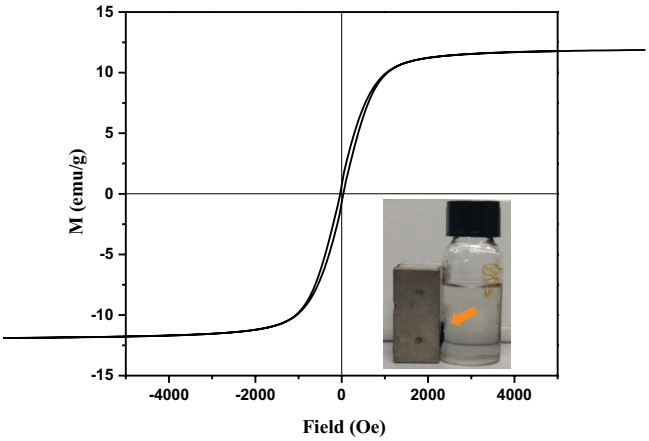

Fig. 7. Magnetization curve of M-FegN/G and its optical photo (inset) in the water solution after separated by a magnet.

FegN/SBA-15 shifted to a lower energy position, suggesting a longer Fe–N bond length weakening the ligand effect and therefore causing a catalytic ability decrease compared with FegN/G [29,31]. This effect was probably caused by the strong attraction of tetrahedral aluminium in the SBA-15 skeleton [32]. FegN/AC showed a less symmetric local structure similar to hematin and perhaps was the result of FegN sheet destruction and coordination with oxygen-containing groups of AC. Consequently, the Fe–N bonds reduced as well as the catalytic ability decreased.

3.3. Characterization of the M-FegN/G

For the simplicity of practical operation, magnetic property was next added to the FegN/G catalyst. In the preparation process, both FegN/G and Fe_3O_4 were adsorbed by the CS–Fe hydrogel and finally encapsulated in the polymer matrix after the cross-link by Na_2SO_4 [18]. Compared with FegN/G, the particle size of M-FegN/G has no obvious change and keeps at dozens of micrometers (Figs. S3 and S4). However, the magnifying images show the successful combination with Fe_3O_4, as small spheres which can be recognized as Fe_3O_4 were adhered to big particles. According to the EDS results in Table S1, the N element content dropped from 26.76% to 15.20% after the magnetic modification, thus the FegN/G composition in the obtained M-FegN/G can be calculated as 56.8% (the N content in chitosan-Fe was not detected by EDS). In addition, new peaks emerged at the FTIR spectra as shown in Fig. S5(a), such as 581 and 1,094 cm^{-1} which associate the vibration of Fe–O bond in Fe_3O_4 and the asymmetrical stretch of C–O–C groups in chitosan. And XRD spectra also confirmed the successful magnetic modification (Fig. S5(b)).

Magnetic properties of the M-FegN/G were characterized by the hysteresis loop and shown in Fig. 7. The saturation magnetization of the composite is 11.7 emu/g, indicating a significant ferromagnetic property. The inset picture in Fig. 7 clearly shows that the catalyst can be easily removed from water by a magnet. Besides, due to the low remnant magnetization of 0.70 emu/g, it can also be easily re-dispersed to water for reuse after separating [33].

3.4. BPA degradation by M-FegN/G

When the dosage of M-FegN/G was 0.8 g/L, the removal efficiency of BPA in 1 h was only 87.6% (Fig. 8(a)), which is lower than FegN/G. And it proved that 99.9% removal can be obtained when the dosage increased to 1.6 g/L. Considering the efficiency, 1.6 g/L was chosen as the optimal dosage in the following experiments. The decrease in catalytic ability compared with FegN/G is owing to the reducing active constituent loading, as the combined CS–Fe and Fe_3O_4 are incompetent to remove BPA (Fig. 8(b)). However, these inactive species helps the catalyst particles to be collected easily by a magnet. After magnetic separation, the catalyst underwent a 7-cycle reuse experiment. In this process, the removal efficiency of BPA slightly decreased to 87.4% (Fig. 8(c)) and the leaching Fe contents were all lower than the limitation of 2 ppm in EU and US [34], indicating a good reusability and stability.

From Fig. 8(b), we can see that only 6.93% of BPA can be removed through the adsorption of M-FegN/G, which in turn suggests that the whole removal process when using H_2O_2 was mainly dominated by oxidation. Further analysis confirmed this oxidation was induced by the hydroxyl radicals, as the ESR spectra in Fig. 9 displayed a typical 4-fold peak of DMPO-·OH with an intensity ratio of 1:2:2:1 in aqueous solution but nothing in methanol solution [35]. And ESR spectra also proved that Fe_3O_4 and CS–Fe can contribute a small part to the ·OH production. Based on these results, we can deduce that the reaction mechanism involves the Fe(III)/Fe(II) cycles happened mainly on the Fe–N centers of the catalyst. Compared with common Fenton reactions, this electron transfer is accelerated by the coordination with g-C_3N_4 and the interaction with graphite, leading to the high catalytic activity of M-FegN/G. Once the ·OH was produced, BPA in the solution could be attacked, yielding various intermediates like aliphatic acids and finally mineralized to CO_2 and H_2O [36]. The TOC removal in 1 h was only 15.1%; however, aromatic organics were greatly

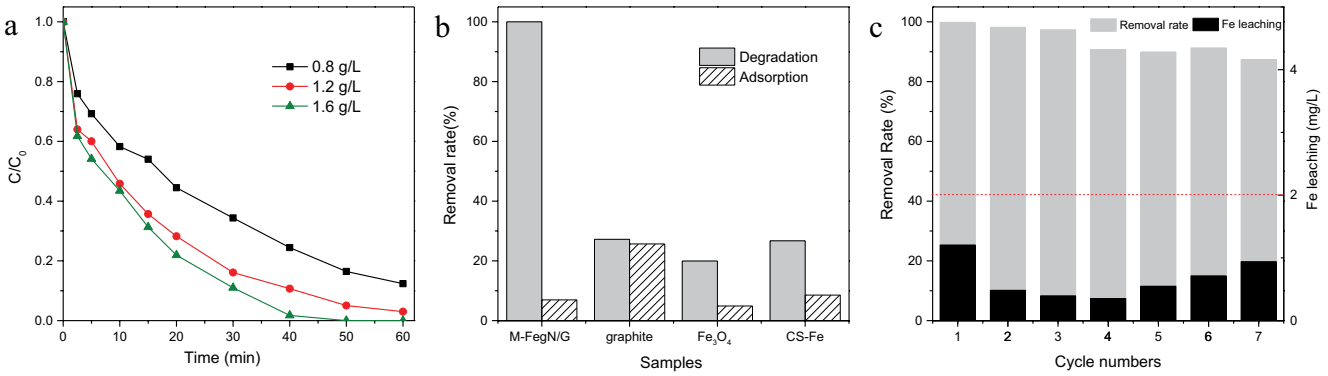

Fig. 8. (a) Time profiles of BPA removal by M-FegN/G under different catalyst dosages, (b) the comparison of BPA removal rate by different samples through degradation (40 mM H_2O_2) and adsorption (no H_2O_2 addition), and (c) BPA removal rates at 7 cycles of reuse and the corresponding concentration of leaching Fe in the solution (BPA 20 mg/L, pH = 6.8, catalyst 1.6 g/L, H_2O_2 40 mM 1 h, 25°C).

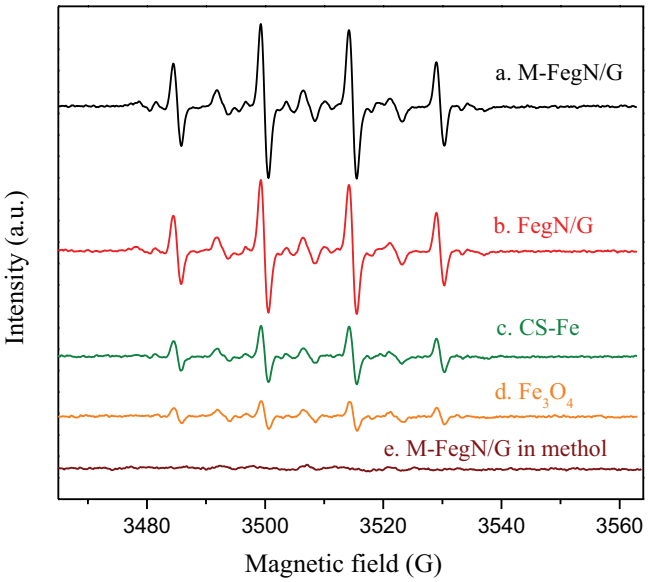

Fig. 9. DMPO spin-trapping ESR spectra reacted (a)–(d) in aqueous solution by different samples and (e) in methanol solution by M-FegN (catalyst 0.8 g/L, H_2O_2 40 mM). The samples were taken out at 5 min and immediately 0.18M DMPO was added for analysis.

reduced according to HPLC spectra in Fig. S6. What's more, formic acid was much produced and finally accumulated to 0.52 mmol/L (original BPA concentration was 0.088 mmol/L, which means 39.4% of original C atoms have turned to formic acid), indicating that the organics after this Fenton-like reaction catalyzed by the M-FegN/G were more biologically degradable.

4. Conclusions

This study prepared a FegN/G composite which exhibited excellent catalytic ability for the Fenton-like reaction. Compared with AC and SBA-15, the addition of the graphite not only increased the active Fe–N centers for the catalyst but also promoted the electron transfer through the strong electron coupling. And then magnetic FegN/G was fabricated through a simple coprecipitation method using Fe_3O_4 and chitosan-Fe hydrogel. The obtained catalyst kept a high efficiency for the BPA removal, as well as a good reusability and stability. Hydroxyl radicals were the main active oxygen species in the process, and BPA was thus oxidized and mineralized. More importantly, it can be separated from the solution using a magnet, offering a potential alternative for the Fenton-like catalyst in practical applications.

Acknowledgments

The authors acknowledge financial support from the National Key Research and Development Program of China (2018YFC1800405) and National Natural Science Foundation of China (NSFC, No. 21876150 and 21677124). We also thank the staff at beamlines BL14W1 at the SSRF for providing the beam time and data analysis.

References

[1] X. Wang, K. Maeda, A. Thomas, K. Takanabe, G. Xin, J.M. Carlsson, K. Domen, M. Antonietti, A metal-free polymeric photocatalyst for hydrogen production from water under visible light, Nat. Mater., 8 (2009) 76–80.
[2] W. Liu, J. Ma, C. Shen, Y. Wen, W. Liu, A pH-responsive and magnetically separable dynamic system for efficient removal of highly dilute antibiotics in water, Water Res., 90 (2015) 24–33.
[3] J. Ma, L. Xu, C. Shen, C. Hu, W. Liu, Y. Wen, Fe-N-graphene Al_2O_3/pentlandite from microalgae: high Fenton catalytic efficiency from enhanced Fe^{3+} reduction, Environ. Sci. Technol., 52 (2018) 3608–3614.
[4] X. Chen, J. Zhang, X. Fu, M. Antonietti, X. Wang, Fe-g-C_3N_4-catalyzed oxidation of benzene to phenol using hydrogen peroxide and visible light, J. Am. Chem. Soc., 131 (2009) 11658–11659.
[5] S. Hu, X. Chen, Q. Li, F. Li, Z. Fan, H. Wang, Y. Wang, B. Zheng, G. Wu, Fe^{3+} doping promoted N_2 photofixation ability of honeycombed graphitic carbon nitride: the experimental and density functional theory simulation analysis, Appl. Catal., B, 201 (2017) 58–69.
[6] Q. Liu, J. Zhang, Graphene supported Co-g-C_3N_4 as a novel metal-macrocyclic electrocatalyst for the oxygen reduction reaction in fuel cells, Langmuir, 29 (2013) 3821–3828.
[7] D. Ghosh, G. Periyasamy, B. Pandey, S.K. Pati, Computational studies on magnetism and the optical properties of transition metal embedded graphitic carbon nitride sheets, J. Mater. Chem. C, 2 (2014) 7943–7951.

[8] Y. Wen, X. Jiang, Pulsed corona discharge-induced reactions of acetophenone in water, Plasma Chem. Plasma Process., 21 (2001) 345–354.
[9] J. Ma, Q. Yang, Y. Wen, W. Liu, Fe-g-C_3N_4/graphitized mesoporous carbon composite as an effective Fenton-like catalyst in a wide pH range, Appl. Catal., B, 201 (2017) 232–240.
[10] X. Li, W. Liu, J. Ma, Y. Wen, Z. Wu, High catalytic activity of magnetic FeOx/NiOy/SBA-15: the role of Ni in the bimetallic oxides at the nanometer level, Appl. Catal., B, 179 (2015) 239–248.
[11] M. Zhang, X. Xie, M. Tang, C.S. Criddle, Y. Cui, S.X. Wang, Magnetically ultraresponsive nanoscavengers for next-generation water purification systems, Nat. Commun., 4 (2013) 1866.
[12] L. Xu, X. Li, J. Ma, Y. Wen, W. Liu, Nano-MnO_x on activated carbon prepared by hydrothermal process for fast and highly efficient degradation of azo dyes, Appl. Catal. A Gen., 485 (2014) 91–98.
[13] E. Antolini, Carbon supports for low-temperature fuel cell catalysts, Appl. Catal. A Gen., 88 (2009) 1–24.
[14] Z. Chen, J. Wang, H. Chen, Y. Wen, W. Liu, Enantioselective phytotoxicity of dichlorprop to *Arabidopsis thaliana*: the effect of cytochrome P450 enzymes and the role of Fe, Environ. Sci. Technol., 51 (2017) 12007–12015.
[15] F. Lücking, H. Köser, M. Jank, A. Ritter, Iron powder, graphite and activated carbon as catalysts for the oxidation of 4-chlorophenol with hydrogen peroxide in aqueous solution, Water Res., 32 (1998) 2607–2614.
[16] Y. Li, M. Guo, S. Yin, L. Chen, Y. Zhou, R. Qiu, C. Au, Graphite as a highly efficient and stable catalyst for the production of lactones, Carbon, 55 (2013) 269–275.
[17] V. Fuster, F.J. Castro, H. Troiani, G. Urretavizcaya, Characterization of graphite catalytic effect in reactively ball-milled MgH_2–C and Mg–C composites, Int. J. Hydrogen Energy, 36 (2011) 9051–9061.
[18] J. Ma, Q. Yang, D. Xu, X. Zeng, Y. Wen, W. Liu, Efficient removal of antibiotics in a fluidized bed reactor by facile fabricated magnetic powdered activated carbon, Environ. Sci. Pollut. Res. Int., 24 (2016) 3820–3828.
[19] I. Bautista-Toledo, M.A. Ferro-García, J. Rivera-Utrilla, C. Moreno-Castilla, F.J. Vegas Fernández, Bisphenol A removal from water by activated carbon. Effects of carbon characteristics and solution chemistry, Environ. Sci. Technol., 39 (2005) 6246–6250.
[20] Y. Deng, D. Qi, C. Deng, X. Zhang, D. Zhao, Superparamagnetic high-magnetization microspheres with an Fe_3O_4@SiO_2 core and perpendicularly aligned mesoporous SiO_2 shell for removal of microcystins, J. Am. Chem. Soc., 130 (2008) 28–29.
[21] C. Jiang, S. Pang, J. Ma, W. Xie, Y. Zou, Spectrophotometric determination of hydrogen peroxide in Fenton reaction with titanium oxalate, China Water Wastewater, 22 (2006) 88–91.
[22] L. Lyu, L. Zhang, C. Hu, Galvanic-like cells produced by negative charge nonuniformity of lattice oxygen on d-TiCuAl-SiO_2 nanospheres for enhancement of Fenton-catalytic efficiency, Environ. Sci. Nano, 3 (2016) 1483–1492.
[23] Y. Nie, C. Hu, J. Qu, X. Zhao, Photoassisted degradation of endocrine disruptors over CuO_x-FeOOH with H_2O_2 at neutral pH, Appl. Catal., B, 87 (2009) 30–36.
[24] A. Hiroki, J.A. LaVerne, Decomposition of hydrogen peroxide at water-ceramic oxide interfaces, J. Phys. Chem. B, 109 (2005) 3364–3370.
[25] L.B. Khalil, B.S. Girgis, T.A. Tawfik, Decomposition of H_2O_2 on activated carbon obtained from olive stones, J. Chem. Technol. Biotechnol., 76 (2001) 1132–1140.
[26] S. Liu, B. Xiao, L. Feng, S. Zhou, Z. Chen, C. Liu, F. Chen, Z. Wu, N. Xu, W.C. Oh, Z.D. Meng, Graphene oxide enhances the Fenton-like photocatalytic activity of nickel ferrite for degradation of dyes under visible light irradiation, Carbon, 64 (2013) 197–206.
[27] N.A. Zubir, C. Yacou, J. Motuzas, X.W. Zhang, J.C.D. da Costa, Structural and functional investigation of graphene oxide-Fe_3O_4 nanocomposites for the heterogeneous Fenton-like reaction, Sci. Rep., 4 (2014) 4594.
[28] J. Zhou, P.N. Duchesne, Y. Hu, J. Wang, P. Zhang, Y. Li, T. Regier, H. Dai, Fe–N bonding in a carbon nanotube–graphene complex for oxygen reduction: an XAS study, Phys. Chem. Chem. Phys., 16 (2014) 15787–15791.
[29] Q. Jia, N. Ramaswamy, H. Hafiz, U. Tylus, K. Strickland, G. Wu, B. Barbiellini, A. Bansil, E.F. Holby, P. Zelenay, Experimental observation of redox-induced Fe–N switching behavior as a determinant role for oxygen reduction activity, ACS Nano, 9 (2015) 12496–12505.
[30] X. Chen, D. Deng, X. Pan, Y. Hu, X. Bao, N-doped graphene as an electron donor of iron catalysts for CO hydrogenation to light olefins, Chem. Commun., 51 (2015) 217–220.
[31] A. Bianconi, M. Dell'Ariccia, P.J. Durham, J.B. Pendry, Multiple-scattering resonances and structural effects in the x-ray-absorption near-edge spectra of Fe II and Fe III hexacyanide complexes, Phys. Rev. B, 26 (1982) 6502.
[32] H. Lim, J. Lee, S. Jin, J. Kim, J. Yoon, T. Hyeon, Highly active heterogeneous Fenton catalyst using iron oxide nanoparticles immobilized in alumina coated mesoporous silica, Chem. Commun., 4 (2006) 463–465.
[33] T.D. Nguyen, N.H. Phan, M.H. Do, K.T. Ngo, Magnetic Fe_2MO_4 (M: Fe, Mn) activated carbons: fabrication, characterization and heterogeneous Fenton oxidation of methyl orange, J. Hazard. Mater., 185 (2011) 653–661.
[34] X. Li, X. Liu, L. Xu, Y. Wen, J. Ma, Z. Wu, Highly dispersed Pd/PdO/Fe_2O_3 nanoparticles in SBA-15 for Fenton-like processes: confinement and synergistic effects, Appl. Catal., B, 165 (2015) 79–86.
[35] Z. Matuszak, K.J. Reszka, C.F. Chignell, Reaction of melatonin and related indoles with hydroxyl radicals: EPR and spin trapping investigations, Free Radical Biol. Med., 23 (1997) 367–372.
[36] L. Lyu, L. Zhang, Q. Wang, Y. Nie, C. Hu, Enhanced Fenton catalytic efficiency of γ-Cu–Al_2O_3 by σ-Cu^{2+}–ligand complexes from aromatic pollutant degradation, Environ. Sci. Technol., 49 (2015) 8639–8647.

Supplementary Information

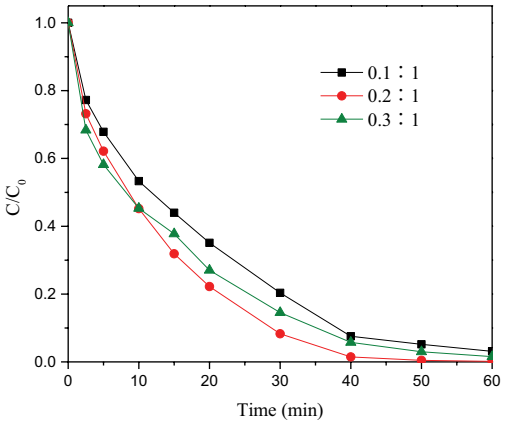

Fig. S1. Time profiles of BPA removal by FegN/G prepared with different graphite dosage (the ratio = graphite:DCD, BPA 20 mg/L, pH = 6.8, FegN/G 0.8 g/L, H_2O_2 40 mM, 25°C).

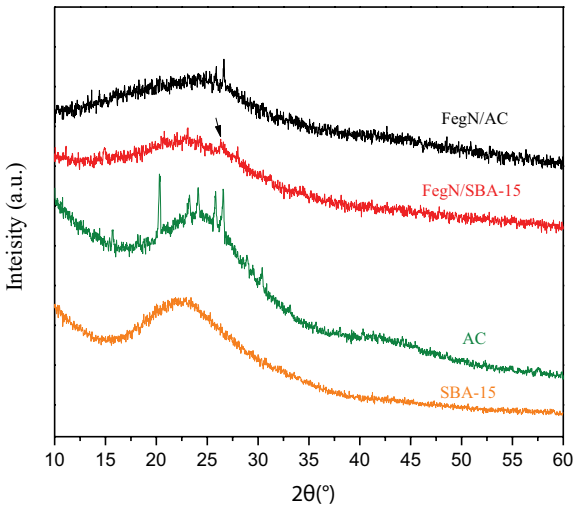

Fig. S2. XRD spectra of the reference samples.

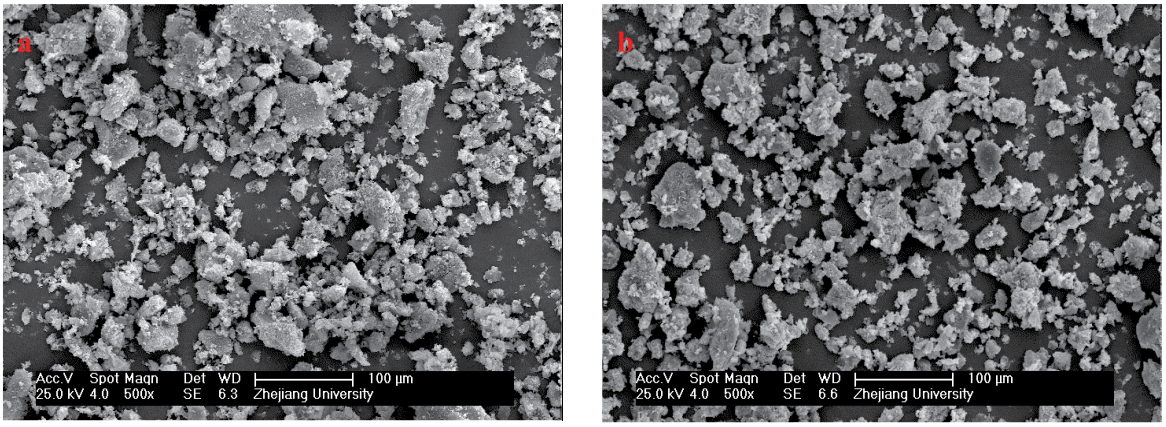

Fig. S3. SEM images of (a) FegN/G and (b) M-FegN/G at low magnification.

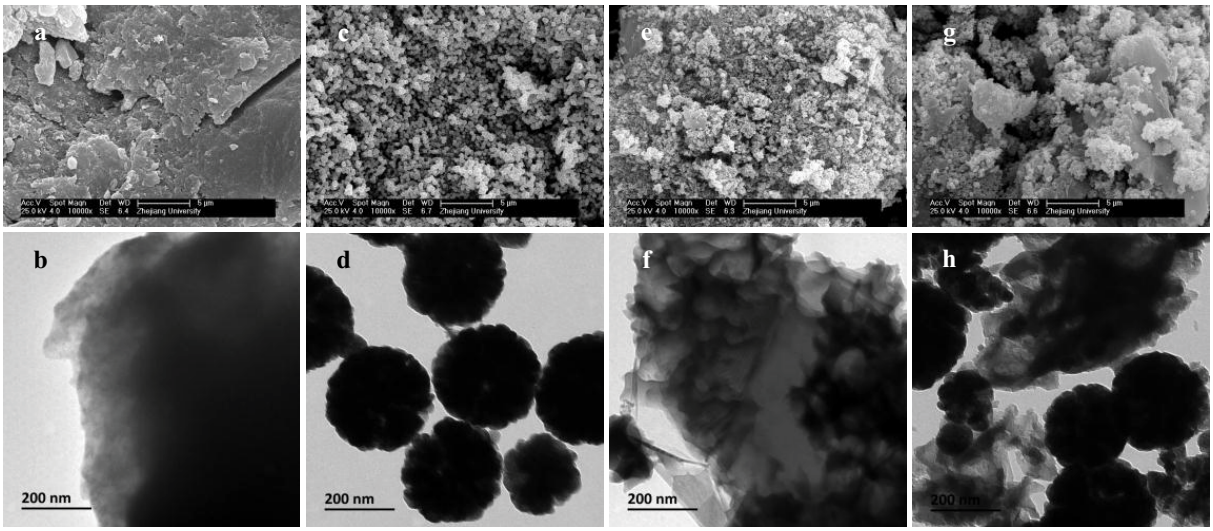

Fig. S4. SEM images (upper) and TEM images (below) of (a),(b) CS–Fe, (c),(d) Fe_3O_4, (e),(f) FegN/G, and (g),(h) M-FegN/G.

Table S1
Element contents of four samples by EDS results

Elements (wt.%)	C	N	O	Fe	S	Cl
CS–Fe	41.39	/	44.59	7.75	5.87	0.41
Fe_3O_4	5.19	/	24.67	70.14	/	/
FegN/G	56.74	26.76	4.14	12.36	/	/
M-FegN/G	51.87	15.20	13.81	17.67	1.45	/

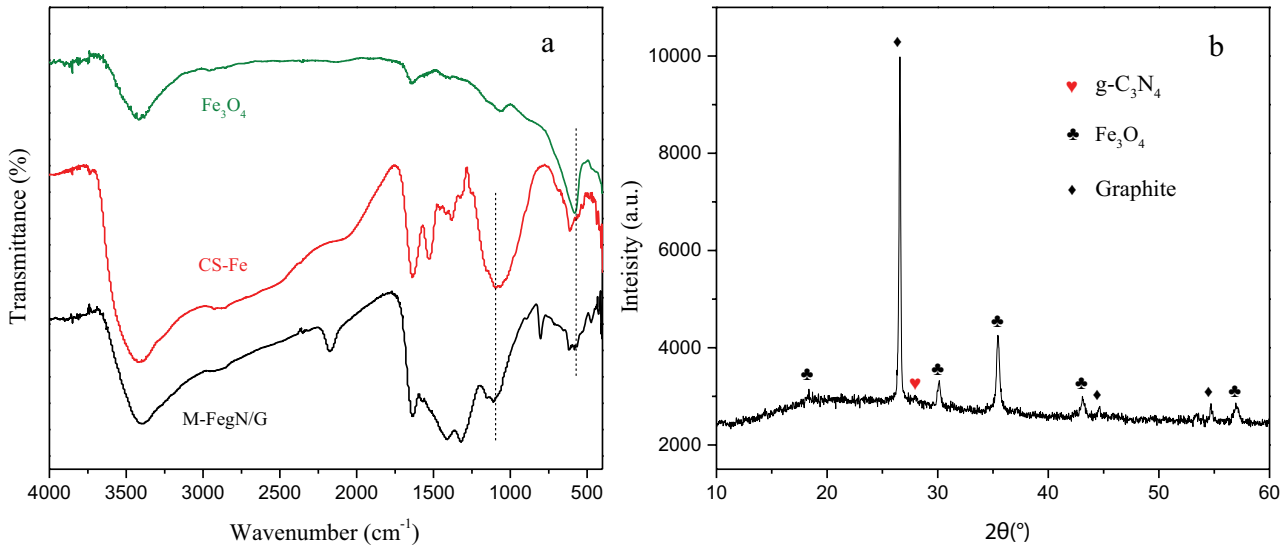

Fig. S5. (a) FTIR spectra of M-FegN/G, CS–Fe, and Fe_3O_4 and (b) XRD spectra of M-FegN/G.

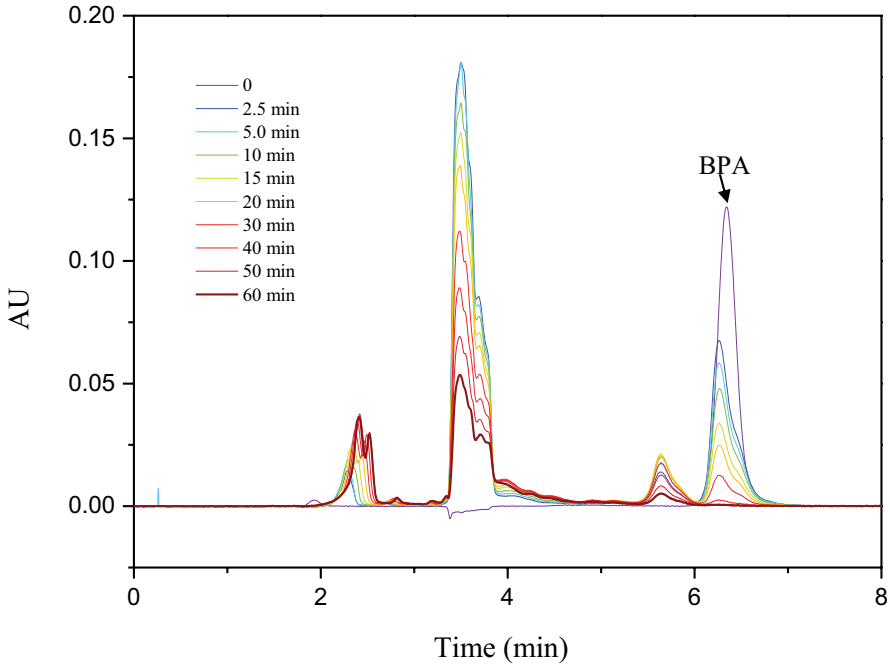

Fig. S6. HPLC-DAD spectra recorded at different time intervals at the BPA degradation process (BPA 20 mg/L, M-FegN/G 1.6 g/L, H_2O_2 40 mM, 25°C).